Inorg. Chem. **2007**, *46*, 11133–11144

Diorganoruthenium Complexes Incorporating Noninnocent $[C_6H_2(CH_2ER_2)_2\text{-}3,5]_2^{2-}$ (E = N, P) Bis-Pincer Bridging Ligands: Synthesis, Spectroelectrochemistry, and DFT Studies

Marcella Gagliardo,[†] Catelijne H. M. Amijs,[†] Martin Lutz,[‡] Anthony L. Spek,[‡,§] Remco W. A. Havenith,[∥,⊥] František Hartl,[*,#] Gerard P. M. van Klink,[†,⊗] and Gerard van Koten[*,†]

Organic Chemistry and Catalysis, Faculty of Science, Utrecht University, Padualaan 8, 3584 CH Utrecht, The Netherlands, Crystal and Structural Chemistry, Faculty of Science, Utrecht University, Padualaan 8, 3584 CH Utrecht, The Netherlands, Theoretical Chemistry Group, Faculty of Science, Utrecht University, Padualaan 8, 3584 CH Utrecht, The Netherlands, and Van't Hoff Institute for Molecular Sciences, University of Amsterdam, Nieuwe Achtergracht 166, 1018 WV Amsterdam, The Netherlands

Received July 27, 2007

The dinuclear complex [(tpy)Ru^{II}(**PCP**–**PCP**)Ru^{II}(tpy)]Cl$_2$ (bridging **PCP**–**PCP** = 3,3′,5,5′-tetrakis(diphenylphosphinomethyl)biphenyl, $[C_6H_2(CH_2PPh_2)_2\text{-}3,5]_2^{2-}$) was prepared via a transcyclometalation reaction of the bis-pincer ligand [**PC(H)P**-**PC(H)P**] and the Ru(II) precursor [Ru(NCN)(tpy)]Cl (NCN = $[C_6H_3(CH_2NMe_2)_2\text{-}2,6]^-$) followed by a reaction with 2,2′:6′,2″-terpyridine (tpy). Electrochemical and spectroscopic properties of [(tpy)Ru^{II}(**PCP**–**PCP**)Ru^{II}(tpy)]Cl$_2$ are compared with those of the closely related [(tpy)Ru^{II}(**NCN**–**NCN**)Ru^{II}(tpy)](PF$_6$)$_2$ (**NCN**–**NCN** = $[C_6H_2(CH_2NMe_2)_2\text{-}3,5]_2^{2-}$) obtained by two-electron reduction of [(tpy)Ru^{III}(**NCN**–**NCN**)Ru^{III}(tpy)](PF$_6$)$_4$. The molecular structure of the latter complex has been determined by single-crystal X-ray structure determination. One-electron reduction of [(tpy)Ru^{III}(**NCN**–**NCN**)Ru^{III}(tpy)](PF$_6$)$_4$ and one-electron oxidation of [(tpy)Ru^{II}(**PCP**–**PCP**)Ru^{II}(tpy)]Cl$_2$ yielded the mixed-valence species [(tpy)Ru^{III}(**NCN**–**NCN**)Ru^{II}(tpy)]$^{3+}$ and [(tpy)Ru^{III}(**PCP**–**PCP**)Ru^{II}(tpy)]$^{3+}$, respectively. The comproportionation equilibrium constants K_c (900 and 748 for [(tpy)Ru^{III}(**NCN**–**NCN**)Ru^{III}(tpy)]$^{4+}$ and [(tpy)Ru^{II}(**PCP**–**PCP**)Ru^{II}(tpy)]$^{2+}$, respectively) determined from cyclic voltammetric data reveal comparable stability of the [Ru^{III}–Ru^{II}] state of both complexes. Spectroelectrochemical measurements and near-infrared (NIR) spectroscopy were employed to further characterize the different redox states with special focus on the mixed-valence species and their NIR bands. Analysis of these bands in the framework of Hush theory indicates that the mixed-valence complexes [(tpy)Ru^{III}(**PCP**–**PCP**)Ru^{II}(tpy)]$^{3+}$ and [(tpy)Ru^{III}(**NCN**–**NCN**)Ru^{II}(tpy)]$^{3+}$ belong to strongly coupled borderline Class II/Class III and intrinsically coupled Class III systems, respectively. Preliminary DFT calculations suggest that extensive delocalization of the spin density over the metal centers and the bridging ligand exists. TD-DFT calculations then suggested a substantial MLCT character of the NIR electronic transitions. The results obtained in this study point to a decreased metal–metal electronic interaction accommodated by the double-cyclometalated bis-pincer bridge when strong σ-donor NMe$_2$ groups are replaced by weak σ-donor, π-acceptor PPh$_2$ groups.

Introduction

Experimental and theoretical studies of organometallic compounds containing two or more multivalent metal centers covalently linked by π-conjugated organic spacer groups are a topic of active research.[1] Such systems are exploited to study the degree of electronic communication between

* To whom correspondence should be addressed. F.H.: phone, +31-20-525-6450; fax, +31-20-525-6456; e-mail, f.hartl@uva.nl. G.v.K.: phone, +31-30-253-3120; fax: +31-30-252-3615; e-mail, g.vankoten@uu.nl.

† Organic Chemistry and Catalysis, Utrecht University.

‡ Crystal and Structural Chemistry, Utrecht University.

§ To whom crystallographic inquiries should be directed. E-mail: a.l.spek@uu.nl.

∥ Theoretical Chemistry Group, Utrecht University. Present address: Electronic Structure of Materials, Institute for Molecules and Materials, Radboud University Nijmegen, Toernooiveld 1, 6525 ED Nijmegen

⊥ To whom correspondence pertaining to theoretical calculations should be addressed. E-mail: r.havenith@science.ru.nl.

University of Amsterdam.

⊗ Present address: DelftChemTech, Faculty of Applied Sciences, Delft University of Technology, Julianalaan 136, 2628 BL Delft, The Netherlands.

10.1021/ic701501q CCC: $37.00
Published on Web 12/01/2007

Scheme 1. Synthesis of the Dinuclear Complexes Containing the Double-Cyclometalated Bis-Pincer Bridging Ligand [**NCN**−**NCN**][a]

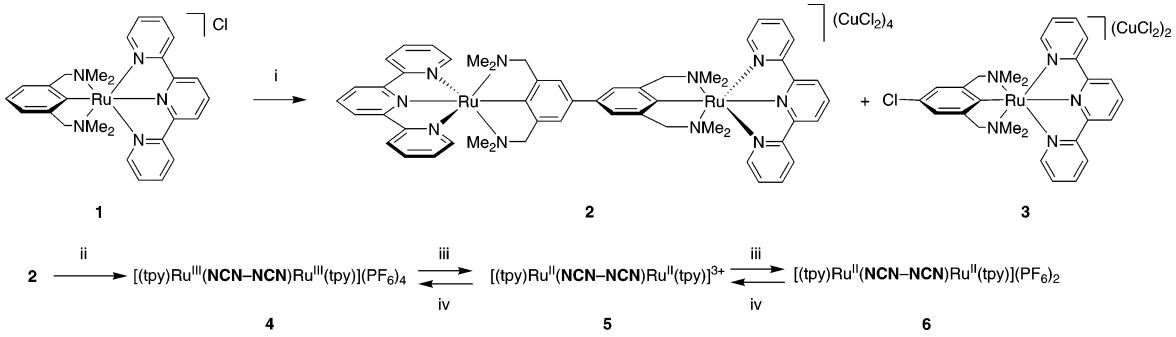

[a] Reagents and experimental conditions: (i) 2.5 equiv of $CuCl_2$, MeOH, reflux, 5 h; (ii) NH_4PF_6, H_2O, rt; (iii) $N_2H_4 \cdot H_2O$, H_2O/MeCN, rt; (iv) $[Cp_2Fe]PF_6$, H_2O/MeCN, rt.

metallic redox units and identify potential candidates for diverse materials applications, for example, in the emerging field of molecular electronics, telecommunications, and aerospace.[2]

There are several factors affecting the degree of electronic coupling and thereby the metal−metal interactions and electron-transfer properties in such species. The nature of the metallic termini, the bridging and ancillary ligands, and the solvent play a crucial role. In the past decades, a plethora of diverse diruthenium systems $[RuL_x](\mu\text{-bridge})[RuL_x]$ were synthesized and studied.[3] The fundamental question about the role of the π-conjugated bridging ligand in the electronic communication between the metal centers has evoked an increasing number of spectroelectrochemical studies aimed at spectroscopic characterization of these homometallic species in several electrochemically accessible redox states with special focus on the so-called mixed-valence (Ru(II)/Ru(III)) state. Among these systems, examples of organometallic dinuclear complexes featuring unsaturated polyyndiyl (−C≡C−)$_n$, polyenediyl (−CH=CH−)$_n$, aryldiethynyl (−C≡C(Ar)C≡C−), aryldiethenyl (−CH=CH(Ar)CH=CH−), and cyanoacetylide (−C≡C−C≡N···) ligands are of special interest as their oxidation is often significantly localized also on the bridging ligand.[1b,4] Given the substantial contribution of the noninnocent bridging ligand to the complex HOMO (the target orbital for the oxidation), the interpretation of the mixed-valence state on grounds of the classical Hush theory and the Robin and Day classification scheme becomes ambiguous. Obviously, attempts to address the issue of the extensive mixing of metal and ligand orbitals and electronic coupling in the mixed-valence redox state require a thorough analysis of experimental (electrochemical, spectral, and magnetic) data and support from quantum chemical calculations being aware of their limitations (DFT).

Apart from the unsaturated carbon chains as bridging ligands, the complexes $[(ttpy)Ru^{II}(\mathbf{tpbp})_2Ru^{II}(ttpy)](PF_6)_2$ (ttpy = 4′-tolyl-2,2′:6′,2″-terpyridine; **tpbp**H_2 = 3,3′,5,5′-tetrapyridylbiphenyl)[5] and $[(tpy)Ru^{III}(\mathbf{NCN}-\mathbf{NCN})Ru^{III}(tpy)](PF_6)_4$ (**4**, Scheme 1)[6] featuring strong σ-donor, dianionic carbon-ligating bridging ligands (Chart 1), have also been reported in the literature as precursors of mixed-valence complexes absorbing strongly in the NIR region: $K_c = 600$, NIR band at 1620 nm, and $\epsilon = 26\,000\ M^{-1}\ cm^{-1}$ and $K_c = 1100$, NIR band at 1875 nm, and $\epsilon = 33\,000\ M^{-1}\ cm^{-1}$. On the basis of these data, the electronic coupling between the ruthenium centers in $[(tpy)Ru^{III}(\mathbf{NCN}-\mathbf{NCN})Ru^{II}(tpy)]^{3+}$ is stronger compared to that in $[(ttpy)Ru^{III}(\mathbf{tpbp})Ru^{II}(ttpy)]^{3+}$. Thus, the extent of electronic communication between the ruthenium centers in such systems can be tuned by varying the electron-donating ability of the double-cyclometalated bis-pincer bridge. With the aim to address the role of the electronic properties of this bridging ligand in the metal−metal interaction and the associated redox and spectroscopic behavior we focused our efforts on the properties of the analogous mixed-valence complex $[(tpy)Ru^{III}(\mathbf{PCP}-\mathbf{PCP})Ru^{II}(tpy)]^{3+}$ (**17** in Scheme 3, vide infra) obtained by one-electron oxidation of the novel dinuclear precursor $[(tpy)Ru^{II}(\mathbf{PCP}-\mathbf{PCP})Ru^{II}(tpy)]Cl_2$ (**16**). The latter complex was synthesized by a selective metalation of the bis-pincer ligand [**PC(H)P**−**PC(H)P**] via a transcyclometalation procedure followed by reaction with tpy. As part of the spectroelectrochemical study, the near-infrared absorption spectrum of the mixed-valence species $[(tpy)Ru^{III}(\mathbf{PCP}-\mathbf{PCP})Ru^{II}(tpy)]^{3+}$ (**17**) was recorded and compared to that of $[(tpy)Ru^{III}(\mathbf{NCN}-\mathbf{NCN})Ru^{II}(tpy)]^{3+}$ (**5**). The extent to which replacement of

(1) (a) *Molecular Switches*; Feringa, B. L., Ed.; Wiley-VCH: Weinheim, 2001. (b) Ren, T. *Organometallics* **2005**, *24*, 4854−4870.

(2) (a) *Infrared Optical Circuits and Components: Design and Applications*; Murphy, E. J., Ed.; Marcel Dekker: New York, 1999. (b) Fabian, J.; Nakamura, I.; Matsuoka, M. *Chem. Rev.* **1992**, *92*, 1197−1226. (c) Chandrasekhar, P.; Zay, B. J.; Birur, G. C.; Rawal, S.; Pierson, E. A.; Kauder, L.; Swanson, T. *Adv. Funct. Mater*. **2002**, *12*, 95−103. (d) Ward, M. D.; McCleverty, J. A. *J. Chem. Soc., Dalton Trans*. **2002**, 275−288 and references cited therein.

(3) Representative examples: (a) Rillema, D. P.; Mack, K. B. *Inorg. Chem.* **1982**, *21*, 3849−3854. (b) Richardson, D. E.; Taube, H. *J. Am. Chem. Soc*. **1983**, *105*, 40−51. (c) Goldsby, K. A.; Meyer, T. J. *Inorg. Chem*. **1984**, *23*, 3002−3010. (c) Hupp, J. T. *J. Am. Chem. Soc*. **1990**, *112*, 1563−1565. (d) Salsman, J.; Kubiak, C. P. *J. Am. Chem. Soc*. **2005**, *127*, 2382−2383. (e) Jose, D. A.; Shukla, A. D.; Kumar, D. K.; Ganguly, B.; Das, A.; Ramakrishna, G.; Palit, D. K.; Ghosh, H. N. *Inorg. Chem*. **2005**, *44*, 2414−2425. (f) Fabrizi De Biani, F.; Dei, A.; Sangregorio C.; Sorace L. *J. Chem. Soc., Dalton Trans.* **2005**, 3868−3873. (g) D'Alessandro, D. M.; Topley, A. C.; Davies, M. S.; Keene, F. R. *Chem. Eur. J.* **2006**, *12*, 4873−4884.

(4) (a) Cordiner, R. L.; Smith, M. E.; Batsanov, A. S.; Albesa-Jové, D.; Hartl, F.; Howard, J. A. K.; Low, P. J. *Inorg. Chim. Acta* **2006**, *359*, 946−961. (b) Gao, L.-B.; Liu, S.-H.; Zhang, L.-Y.; Shi, L.-X.; Chen, Z.-N. *Organometallics* **2006**, *25*, 506−512. (c) Klein, A.; Lavastre, O.; Fiedler, J. *Organometallics* **2006**, *25*, 635−643. (d) Roberts, R. L.; LeGuedennic, B.; Halet, J.-F.; Hartl, F.; Howard, J. A. K.; Low, P. J. Manuscript in preparation. (e) Maurer, J.; Winter, R. F.; Sarkar, B.; Záliš, S. *J. Solid State Chem.* **2005**, *9*, 738−749.

Scheme 2. Synthesis of the Bis-Pincer Ligand **13**[a]

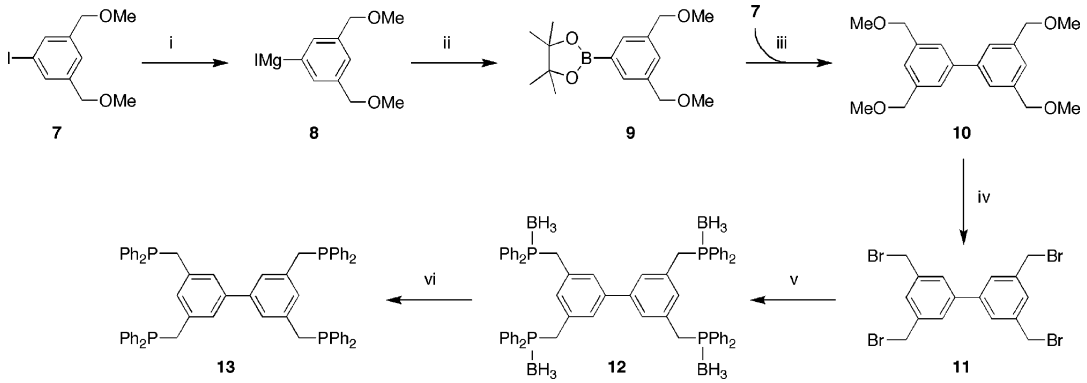

[a] Reagents and conditions: (i) (a) 2 equiv of Mg, THF, rt, 3 h; (b) reflux, ca. 15 h; (ii) $B(OMe)_3$, pinacol, AcOH, rt, 1 h; (iii) **7**, Na_2CO_3, [$PdCl_2$(dppf)], DMF/THF/H_2O (1:1:1 v/v), 50 °C, 15 h; (iv) BF_3·Et_2O, AcBr, CH_2Cl_2, reflux, 18 h; (v) (a) $HPPh_2$·Et_2O, *n*BuLi, THF, −78 °C; (b) rt, 18 h; (vi) HBF_4·Et_2O, rt, 18 h.

Chart 1

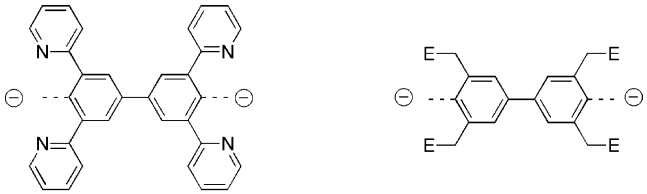

(**tpbp**) (**NCN**–**NCN**), E = NMe_2 (**PCP**–**PCP**), E = PPh_2

the 'hard' NMe_2 donor groups by the 'soft' PPh_2 groups in the dianionic bridging ligand affects the electron-transfer process in both mixed-valence species has been rationalized both in the framework of Hush theory and at a quantum chemical level by DFT and TD-DFT calculations.

Results and Discussion

Structural Characterization of [(tpy)Ru^{III}(NCN−NCN)-Ru^{III}(tpy)]$(PF_6)_4$ (4). Copper(II)-mediated oxidative coupling of the readily accessible 18-electron mononuclear building block [Ru^{II}(NCN)(tpy)]Cl (**1**, Scheme 1) gives the dinuclear 34-electron complex [(tpy)Ru^{III}(**NCN**−**NCN**)Ru^{III}(tpy)]-($CuCl_2$)$_4$ (**2**) in good yield (85%) via a modified literature procedure. The paramagnetic mononuclear *para*-chlorinated compound [Ru^{III}{$C_6H_2(CH_2NMe_2)_2$-2,6-Cl-4}(tpy)]($CuCl_2$)$_2$ (**3**) is formed as a minor product (7%).

Replacement of the two counterions $[CuCl_2]^-$ in **2** by PF_6^- ions yields complex **4**, the structure of which has been determined by single-crystal X-ray structure determination (Figure 1; selected bond lengths and angles are listed in Table 1). The molecular structure of **4** in the crystal is very similar to that of **2**.[6] The two identical ruthenium(III) centers are embedded in a distorted octahedral environment that comprises the terdentate NCN-pincer and tpy ligands coordinated in a meridional arrangement.

Unlike complex **2**, in which two anions $[CuCl_2]^-$ are packed above and below the planar biphenylene bridge (Ar−Ar dihedral angle = 0(4)°) at a distance of ca. 3.5 Å,[6a] the molecular structure of **4** displays a torsion angle of 24.2(4)° between the two phenyl rings (C51−C41−C42−C52). The torsion angle in **4** is slightly smaller than that found in the diruthenium(II) derivative **6** (Scheme 1) (36.0(2)°)[6b] and in a majority of 4,4′-disubstituted (organic) biphenyls (average value of 37°).[7] The other geometrical parameters of **4** and the two-electron-reduced **6** are almost identical. Thus, in both [Ru^{III}−Ru^{III}] and [Ru^{II}−Ru^{II}] species the preferred low-energy solid-state structure has the phenyl rings twisted with respect to each other. These data indicate that the solid-state planarity of the central biphenylene systems in the [Ru^{III}−Ru^{III}] complex **2** is not a result of a favored electronic situation but rather an effect of the crystal packing of the $[CuCl_2]^-$ anions.

The sharp resonances in the aromatic region of the ^{1}H NMR spectrum, associated with the tpy and bridging pincer ligand, reveal that **4** is diamagnetic. Complex **4** is EPR silent both at room temperature and at 77 K in the solid state as well as in MeCN. Its diamagnetic nature has also been confirmed by magnetic susceptibility measurements (SQUID) performed in the temperature range 5−300 K. All these data are indicative of very strong antiferromagnetic coupling[8] between the two Ru(III) centers mediated by the bridging bis(carbon-ligating) biphenylene moiety, which can be ascribed to a significant interaction between the half-filled dπ orbital of the Ru(III) centers with occupied high-lying π orbitals localized on the bridging ligand.[9]

Synthesis of [(tpy)Ru^{II}(PCP−PCP)Ru^{II}(tpy)]Cl_2 (16). The synthetic protocol employed to obtain the dinuclear [Ru^{II}−Ru^{II}] complex **16** in a high yield (ca. 70%) involved preparation of the novel ligand **13** (Scheme 2) followed by

(5) (a) Beley, M.; Collin, J.-P.; Sauvage, J.-P. *Inorg. Chem.* **1993**, *32*, 4539−4543. (b) Patoux, C.; Launay, J.-P.; Beley, M.; Chodorowski-Kimmes, S.; Collin, J.-P.; James, S.; Sauvage, J. -P. *J. Am. Chem. Soc.* **1998**, *120*, 3717−3725.

(6) (a) Sutter, J.-P.; Grove, D. M.; Beley, M.; Collin, J.-P.; Veldman, N.; Spek, A. L.; Sauvage, J.-P.; van Koten, G. *Angew. Chem., Int. Ed. Engl.* **1994**, *33*, 1282−1285. (b) Steenwinkel, P.; Grove, D. M.; Veldman, N.; Spek, A. L.; van Koten, G. *Organometallics* **1998**, *17*, 5647−5655.

(7) (a) Cassalone, G.; Mariani, C.; Mugnoli, A.; Simonetta, M. *Acta Crystallogr., Sect. B* **1969**, *25*, 1741−1750. (b) Iwamoto, T.; Miyoshi, T.; Sasaki, Y. *Acta Crystallogr., Sect. B* **1974**, *30*, 292−295. (c) Brock, C. P.; Kuo, M.-S.; Levy, H. A. *Acta Crystallogr., Sect. B* **1978**, *34*, 981−985. (d) Naae, D. G. *Acta Crystallogr., Sect. B* **1979**, *35*, 2765−2768.

(8) Carlin, R. L. *Magneto Chemistry*; Springer-Verlag: Berlin, 1986.

(9) Kahn, O. In *Magneto-Structural Correlations in Exchange Coupled Systems*; Willet, R. D., Gatteschi, D., Kahn, O., Eds.; NATO ASI Series 37; D. Riedel Publishing Co.: Dordrecht, 1984.

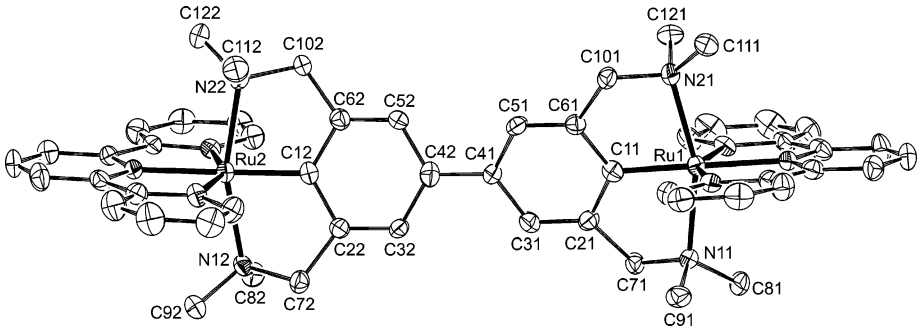

Figure 1. Displacement ellipsoid plot of complex **4** (50% probability level). Hydrogen atoms, the PF_6^- counterions, and disordered solvent molecules have been omitted for clarity.

Scheme 3. Synthesis of the Dinuclear Complexes Containing the Biscyclometalated Bis-Pincer Bridging Ligand [**PCP**−**PCP**][a]

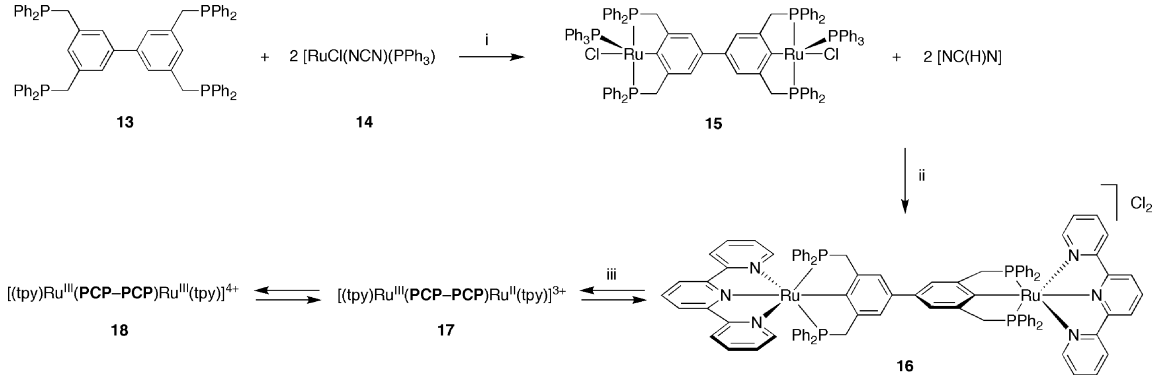

[a] Reagents and conditions: (i) C_6H_6, reflux, 2 d; (ii) tpy, MeOH; (iii) $[Ce(OTf)_4]$, MeCN, rt.

Table 1. Selected Bond Lengths and Angles and Torsion Angles in Complex **4**

bond lengths [Å]			
Ru1−C11	1.914(3)	Ru2−C12	1.913(3)
Ru1−N11	2.185(2)	Ru2−N12	2.198(2)
Ru1−N21	2.208(2)	Ru2−N22	2.194(2)
Ru1−N31	2.084(2)	Ru2−N32	2.087(2)
Ru1−N41	2.087(2)	Ru2−N42	2.086(2)
Ru1-N51	2.087(2)	Ru2−N52	2.095(2)
C41−C42	1.459(4)		
bond angles [deg]			
C11−Ru1−N41	177.34(10)	C12−Ru2−N42	177.65(10)
N11−Ru1−N21	160.21(8)	N12−Ru2−N22	160.78(8)
N31−Ru1−N51	152.61(9)	N32−Ru2−N52	152.96(9)
torsion angles [deg]			
Ru1−N11−C71−C21	−34.8(2)	Ru2−N12−C72−C22	−32.6(2)
Ru1−N21−C101−C61	−36.7(2)	Ru2−N22−C102−C62	−36.1(3)
C31−C41−C42−C32	24.7(4)	C51−C41−C42−C52	24.2(4)
C31−C41−C42−C52	−156.0(3)	C51−C41−C42−C32	−155.1(3)

introduction of ruthenium metal centers via a transcyclometalation (TCM) reaction[10] to give the dinuclear complex **15** and its subsequent reaction with tpy to give **16** (Scheme 3). In the synthesis of **13** (Scheme 2), 3,5-bis(methoxymethyl)-iodobenzene (**7**) was reacted with 2 equiv of Mg in THF. The Grignard reagent **8** was then subsequently treated in THF with $B(OMe)_3$ and pinacol to form **9**, which is highly soluble in organic solvents and, in contrast to the majority of boronic acids, insoluble in water. A Pd-catalyzed Suzuki cross-coupling between the pinacol-protected boronic acid **9** and **7** gave **10** in high yield. This sequence was especially convenient because of the high yields and mild reaction conditions applied. The ease of this preparation is another advantage as none of these steps requires tedious purification procedures. In addition, unreacted **7** can be easily recovered and reused. Replacement of the MeO groups in **10** by Br substituents was carried out, following the procedure reported by Dijkstra et al.[11] Thus, reaction of **10** with the Lewis acid $BF_3{\cdot}Et_2O$ and acetyl bromide in CH_2Cl_2 at reflux gave **11** in a good yield. Ligand **13** was obtained applying a two-step procedure previously reported for the preparation of multi-PCP pincer ligand systems.[11] Treatment of **11** in situ with $Li-PPh_2(BH_3)$ gave **12**, which was subsequently deprotected with $HBF_4{\cdot}OEt_2$, yielded bis-pincer ligand **13** as a sticky white solid.

Mixing **13** with two equivalents of ruthenium precursor **14** ($[RuCl(NCN)(PPh_3)]$,[12] NCN = $[C_6H_3(CH_2NMe_2)_2\text{-}2,6]^-$) resulted in selective transcyclometalation of the two PCP

(10) (a) Dani, P.; Karlen, T.; Gossage, R. A.; Smeets, W. J. J.; Spek, A. L.; van Koten, G. *J. Am. Chem. Soc.* **1997**, *119*, 11317−11318. (b) Albrecht, M.; Dani, P.; Lutz, M.; Spek, A. L.; van Koten, G. *J. Am. Chem. Soc.* **2000**, *122*, 11822−11833. (c) Dani, P.; Albrecht, M.; van Klink, G. P. M.; van Koten, G. *Organometallics* **2000**, *19*, 4468−4476.

(11) (a) Dijkstra, H. P.; Steenwinkel, P.; Grove, D. M.; Lutz, M.; Spek, A. L.; van Koten, G. *Angew. Chem., Int. Ed.* **1999**, *38*, 2186−2188. (b) Dijkstra, H. P.; Meijer, M. D.; Patel, R.; Kreiter, R.; van Klink, G. P. M.; Lutz, M.; Spek, A. L.; Canty, A. J.; van Koten, G. *Organometallics* **2001**, *20*, 3159−3168.

(12) Sutter, J.-P.; James, S. L.; Steenwinkel, P.; Karlen, T.; Grove, D. M.; Veldman, N.; Smeets, W. J. J.; Spek, A. L.; van Koten, G. *Organometallics* **1996**, *15*, 941−948.

Scheme 4. Synthesis of the Ligand **21** and Dinuclear Complexes **23** and **6**[a]

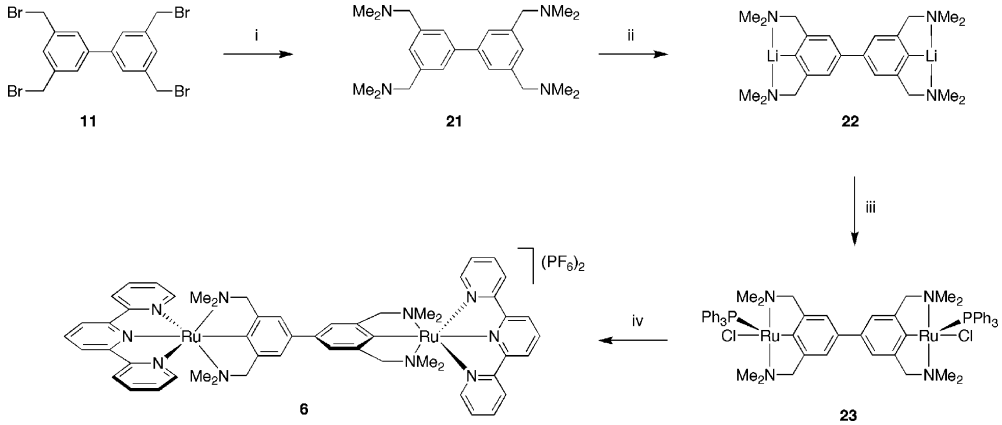

[a] Reagents and conditions: (i) $HNMe_2$, CH_2Cl_2, rt, 3 h; (ii) (a) 2.3 equiv of *t*BuLi, Et_2O, −78 °C; (b) rt, 14 h; (iii) [$RuCl_2(PPh_3)$], THF, rt, 5 h; (iv) (a) tpy, MeOH; (b) excess NH_4PF_6.

sites of ligand **13** and concomitant formation of two equivalents of the bis(aminoarene) NC(H)N-pincer ligand (Scheme 3). The ^{1}H NMR resonances revealed two equivalent {(PCP)RuCl(PPh_3)} units, which may be attributed to free rotation about the central C−C bond in the **PCP**−**PCP** ligand. In solution, each ruthenium center shows structural features similar to that reported for the mononuclear species [RuCl(PCP)(PPh_3)][13] (PCP = [$C_6H_3(CH_2PPh_2)_2$-2,6]$^-$), i.e., a distorted square-pyramidal geometry of the ruthenium coordination sphere, with the PPh_3 ligand in the apical position and the two phosphorus centers of the PCP-pincer units together with the C_{ipso} atom forming the base of the square-pyramidal arrangement. The diastereotopic benzylic protons appear as a set of doublets of virtual triplets.[10c] The ^{31}P{^{1}H} NMR spectrum consists of a low-field triplet due to PPh_3 and a doublet due to the two equivalent phosphorus atoms of the PCP-pincer units. Subsequent reaction of the resulting air- and moisture-sensitive dark green complex **15** with two equivalents of tpy gave **16** as an air-stable orange solid in good yield. The ^{1}H and ^{31}P{^{1}H} NMR data of **16**, similar to those recorded for mononuclear [Ru^{II}(PCP)(tpy)]Cl[14] (**19**), reveal a high degree of symmetry in solution. The ^{31}P{^{1}H} NMR spectrum exhibits a single resonance at 43.1 ppm for the equivalent phosphorus centers of each {(tpy)Ru(PCP)} fragment.

Attempts to synthesize the complex [(tpy)Ru^{III}(**PCP**−**PCP**)Ru^{III}(tpy)](PF_6)$_4$ (**18**) by reacting [Ru(PCP)(tpy)]Cl[14] (**19**) with $CuCl_2$ resulted in formation of the mononuclear, *para*-chlorinated complex [Ru^{II}{$C_6H_2(CH_2PPh_2)_2$-2,6-Cl-4}(tpy)](PF_6) (**20**) in ca. 40% yield and desired dinuclear **18** in low yield (15%) only. The yield of **18** remained low even when a large excess of $CuCl_2$ was used and/or the reaction time was prolonged.

The mechanism of the Cu(II)-mediated oxidative C−C coupling, which gave rise to the smooth formation of dinuclear [Ru^{III}−Ru^{III}] species **4**, was not studied in detail, and the intermediates involved in the process have not been isolated or identified so far.[6b] In this proposed mechanism, the first reaction step must involve oxidation of the ruthenium center in mononuclear complex **1** and formation of Cu(I) ions.[6] Oxidation of the ruthenium center results in activation of the *para*-position with respect to the metal center, which reacts further with copper to give complex cluster aggregates involving combinations of Cu(I), Cu(II), and halide ions.[15] Subsequently, as proposed for the arylcopper aggregates,[15] these inner-sphere-activated complexes react with $CuCl_2$ to give unstable {(NCN)Ru^{III}(tpy)}-containing radicals that convert to dinuclear species or *para*-chlorinated species such as **3** and CuCl via a halide ion transfer oxidation pathway.

The reactivity of **19** toward $CuCl_2$ suggests that the enhanced π-accepting character of the phosphorus atoms of the PCP-pincer ligand ($\Delta E_{1/2}$ = 0.16 V vs Fc/Fc$^+$) with respect to the 'hard' σ-donor character of the amine-nitrogen atom of the NCN-pincer ligand in **1** ($\Delta E_{1/2}$ = −0.08 V vs Fc/Fc$^+$) is the main factor controlling the activation of the para position and, in turn, formation of dinuclear complexes in the presence of $CuCl_2$. However, formation of the chloro-functionalized complex **20** indicates that the aryl para position in **19** is somehow activated toward substitution, as observed for a number of cyclometalated Ru(II) compounds.[16]

Replacement of the bromine atoms in **11** by dimethylamino groups[11] gave the bis-pincer ligand precursor 3,3′,5,5′-tetrakis[(dimethylamino)methyl]biphenyl **21** (Scheme 4). The latter compound was already prepared earlier by Lagunas et al. but in a lower yield through a different synthetic procedure.[17] With compound **21** in hand we also attempted the alternative synthesis of the dinuclear complex [(tpy)Ru^{II}(**NCN**−**NCN**)Ru^{II}(tpy)](PF_6)$_2$ (**6**) via transmetalation of the dilithium complex **22** with [$RuCl_2(PPh_3)_3$] to give **23** followed by reaction with tpy (Scheme 4).[12] However, this

(13) (a) Jia, G.; Lee, H. M.; Williams, I. D. *J. Organomet. Chem.* **1997**, *534*, 173−180. (b) Dani, P.; van Klink, G. P. M.; van Koten, G. *Eur. J. Inorg. Chem.* **2000**, *7*, 1465−1470.
(14) Gagliardo, M.; Dijkstra, H. P.; Coppo, P.; De Cola, L.; Lutz, M.; Spek, A. L.; van Klink, G. P. M.; van Koten, G. *Organometallics* **2004**, *23*, 5833−5840.
(15) (a) van Koten, G.; Leusink, A. J.; Noltes, J. G. *J. Organomet. Chem.* **1975**, *84*, 117−127. (b) van Koten, G.; Noltes, J. G. *J. Organomet. Chem.* **1975**, *84*, 419−429.
(16) Gagliardo, M.; Snelders D. J. M.; Chase, P. A.; Klein Gebbink, R. J. M.; van Klink, G. P. M.; van Koten, G. *Angew. Chem., Int. Ed.* **2007**, *46*, 8558−8573.
(17) Lagunas, M.-C.; Gossage, R. A.; Spek, A. L.; van Koten, G. *Organometallics* **1998**, *17*, 731−741.

Table 2. Electrochemical Data for Dinuclear Complexes **6** and **16** and Reference Mononuclear Complexes **1** and **19**

compound	$E_{1/2}$ (V)[a] Ox.1	Ox.2	Red.	K_c[d]
[Ru^{II}(**NCN**)] (**1**)[b]	−0.08		−1.94	
[Ru^{II}(**NCN-NCN**)Ru^{II}] (**6**)[c]	−0.07	−0.25	−1.97	900
[Ru^{II}(**PCP**)] (**19**)[b]	0.16		−1.94	
[Ru^{II}(**PCP-PCP**)Ru^{II}] (**16**)	0.13	−0.04 (0.68)	−1.95	748

[a] Measured at 298 K in butyronitrile containing 10^{-1} M TBAH. Potentials are reported in V vs Fc/Fc^{+}. [b] Reference 14. [c] Reference 6b. [d] Comproportionation equilibrium constant $K_c = \exp(\Delta E_{1/2}/25.69)$ at 298 K.[20] Ox.1 = first formally $Ru^{II/III}$ in mononuclear and dinuclear complexes. Ox.2 = second formally $Ru^{II/III}$ in dinuclear complexes. Red. = tpy/tpy^{-}.

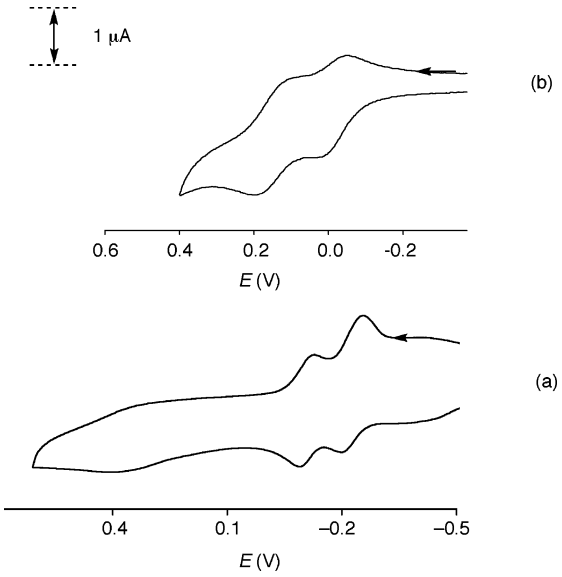

Figure 2. Anodic part of the cyclic voltammograms of **6** (a) and **16** (b). Conditions: Pt disk microelectrode, MeCN/10^{-1} M TBAH, $T = 293$ K, $v = 100$ mV s^{-1}.

protocol gave **6** only in a low yield (15%). The inherently high solubility of **23** and **6** in organic solvents caused a considerable loss of material during the workup procedure. Thus, the Cu(II)-mediated oxidative C−C coupling (Scheme 1) proved to be a more convenient procedure for the preparation of dinuclear organoruthenium−terpyridine complexes containing the bridging **NCN**−**NCN** ligand.

Electrochemistry. The dinuclear complex [(tpy)Ru^{II}-(**PCP**−**PCP**)Ru^{II}(tpy)]$^{2+}$ (**16**) was studied by cyclic voltammetry (CV) and differential pulse voltammetry (DPV) in MeCN at $T = 298$ K. The electrochemical data are summarized in Table 2. Dinuclear complex **4**[6] (i.e., 2e-oxidized **6**) and mononuclear precursors **1**[14] and **19**[14] are also presented for reference purposes.

Similar to **6**, the anodic region of the cyclic voltammogram of **16** (Figure 2b) shows two well-separated one-electron oxidation steps. The current for both peaks is linearly dependent on $\nu_{1/2}$ for the scan rates studied (0.05−1 V s^{-1}) indicating completely reversible, diffusion-controlled processes. Complex **16** is first oxidized to [(tpy)Ru^{III}(**PCP**−**PCP**)Ru^{II}(tpy)]$^{3+}$ (**17**) at 0.13 V vs Fc/Fc^{+} ($\Delta E_p = 0.70$ mV). In the second step, at −0.04 V ($\Delta E_p = 0.68$ mV), the mixed-valence complex is further oxidized to [(tpy)Ru^{III}(**PCP**−**PCP**)Ru^{III}(tpy)]$^{4+}$ (**18**). The oxidation potentials of **16** are significantly higher than those of **6**, reflecting the absence of π-back-donation compared to **PCP**−**PCP**.[14] The oxidation potential of **16** is virtually identical to that reported for mononuclear reference **19**, indicating that the electronic properties of the metal centers in both complexes are very similar. The electronic communication between the metal centers in [(tpy)Ru^{III}(**PCP**−**PCP**)Ru^{II}(tpy)]$^{3+}$ shifts the second oxidation less positively. Despite the π-acceptor character of the **PCP**−**PCP** ligand, the anodic wave separation for complex **17** ($\Delta E_{1/2} = 170$ mV) is slightly smaller compared to **5** ($\Delta E_{1/2} = 180$ mV), corresponding to comproportionation equilibrium constants $K_c = 748$ for **17** and 900 for **5**, respectively. The K_c values reflect the stability of the [Ru^{III}−Ru^{II}] state with respect to disproportionation under the experimental conditions of the voltammetric scan. It is a matter of discussion whether they may also be used to estimate the degree of electronic interaction in the mixed-valence species across the bridging ligand.[18] A cautionary warning on the use of the electrochemical data is required since the voltammetric wave separations are influenced also by other, sometimes even dominant factors (e.g., differences in solvation, supporting electrolyte, repulsion between the two similarly charged metal centers, synergistic factors due to metal−ligand back-bonding) which can modify electrostatic interaction in dinuclear cations.[4e,19] The comparably low values of K_c for **5** and **17** (within the 5% experimental error) are not consistent with a strong interaction between the metal redox sites, in contrast to the large electronic coupling parameters V_{AB} derived from the NIR absorption of the complexes (vide infra). This discrepancy may reflect strong participation of the bridging ligands in the oxidation, as confirmed by the DFT calculations (vide infra).

The cathodic CV scans of **5** and **17** show well-defined reversible waves at −1.97 ($\Delta E_p = 0.60$ mV) and −1.95 V ($\Delta E_p = 0.58$ mV), respectively. On the basis of the DPV peak current intensities, these largely tpy-localized reduction processes are consistent with single-step transfers of two electrons. The reduction potentials of the dinuclear complexes and reference mononuclear compounds **1** and **19** are almost identical. This means that the π^* systems of the ancillary tpy ligands are not affected by the electronic interaction between the metal centers. No cathodic waves were observed for the bridging cyclometalated pincer ligands in **5** and **17** before the solvent discharge.

Electronic Absorption Spectra and UV−vis Spectroelectrochemistry. Table 3 lists the absorption maxima, λ_{max}, and molar absorption coefficients, ϵ_{max}, for dinuclear complexes **4**[6], **6**,[6] and **16** and mononuclear species **1**[14] and **19**.[14] The absorption spectrum of **16** (Figure 3), recorded in MeCN at room temperature, presents features characteristic for the

(18) (a) Hush, N. S. *Electrochim. Acta* **1968**, *13*, 1005−1023. (b) Richardson, D. E.; Taube, H. *Coord. Chem. Rev.* **1984**, *60*, 107−129. (c) Robin, M. B.; Day, P. *Adv. Inorg. Chem. Radiochem.* **1967**, *10*, 247−422. (d) Demadis, K. D.; Hartshorn, C. M.; Meyer, T. J. *Chem. Rev.* **2001**, *101*, 2655−2685. (e) D'Alessandro, D. M.; Keene, F. R. *Chem. Rev.* **2006**, *106*, 2270−2298.

(19) (a) Barriére, F. W. E.; Geiger, W. E. *J. Am. Chem. Soc.* **2006**, *128*, 3980−3989. (b) D'Alessandro, D. M.; Keene, F. R. *Dalton Trans.* **2004**, 3950−3954.

(20) Sutton, J. E.; Sutton, P. M.; Taube, H. *Inorg. Chem.* **1979**, *18*, 1017−1021.

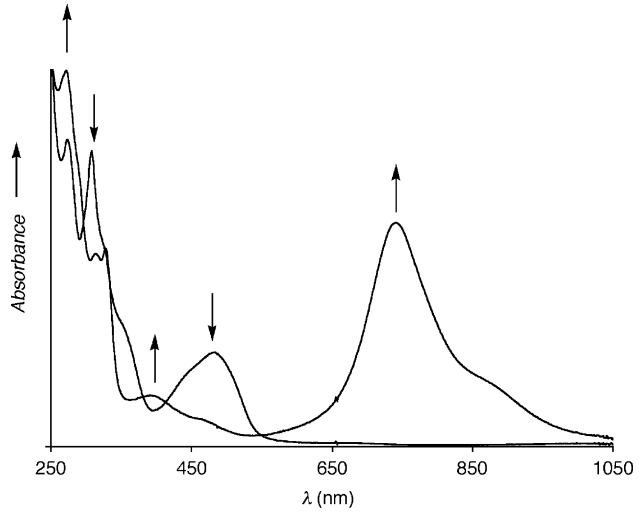

Figure 3. UV−vis spectra recorded before and after the complete two-electron oxidation of complex [(tpy)Ru^{II}(**PCP**−**PCP**)Ru^{II}(tpy)]$^{2+}$ (**16**) to [(tpy)Ru^{III}(**PCP**−**PCP**)Ru^{III}(tpy)]$^{4+}$ (**18**). Conditions: OTTLE cell, $T = 293$ K, MeCN/3 × 10^{-1} M TBAH.

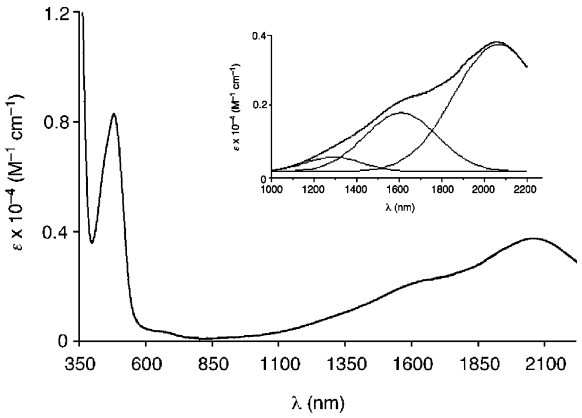

Figure 4. UV−vis−NIR spectrum of the mixed-valence complex [(tpy)-Ru^{III}(**PCP**−**PCP**)Ru^{II}(tpy)]$^{3+}$ (**17**) obtained by chemical oxidation of **16** with [Ce(OTf)$_4$] in MeCN at 293 K. Inset: the deconvoluted NIR band envelope of **17**.

Table 3. UV−vis Absorption Data for the Mononuclear Complexes **1** and **19** and the Dinuclear Complexes **4**, **6**, **16**, and **18**

compound	λ_{max}, nm[a] ($\epsilon_{max} \times 10^4$, $M^{-1}\,cm^{-1}$)
[Ru^{II}(**NCN**)] (**1**)[b]	632 (0.51), 593 (0.53), 524 (0.73), 352 (1.02), 318 (2.09), 280 (3.31)
[Ru^{II}(**NCN-NCN**)Ru^{II}] (**6**)[c]	657(11.70), 306 (3.84), 275 (4.66)
[Ru^{III}(**NCN-NCN**)Ru^{III}] (**4**)[c]	618(1.58), 593 (1.67), 528 (1.81), 377 (3.72), 324 (7.30), 280 (5.95)
[Ru^{II}(**PCP**)] (**19**)[b]	479 (0.51), 307 (2.48), 273 (1.95)
[Ru^{II}(**PCP-PCP**)Ru^{II}] (**16**)	485 (0.90), 363 (1.90), 311 (4.00), 279 (3.56)
[Ru^{III}(**PCP-PCP**)Ru^{III}] (**18**)	896 (1.2), 747 (3.12), 417 (1.4), 317 (3.11), 214 (5.3)

[a] Measured at 298 K in MeCN. [b] Reference 14. [c] Reference 6

class of ruthenium(II)−terpyridine complexes. The UV region is dominated by intense $\pi \rightarrow \pi^*$ intraligand (IL) transitions within the bridging pincer and ancillary terpyridine ligands. The broad absorption bands in the visible region belong to electronic transitions that are assigned a predominant metal-to-ligand charge-transfer (MLCT) character due to spin-allowed dπ(Ru) $\rightarrow \pi^*$(tpy).[21]

The considerable shift to higher energy of the MLCT bands in the UV−vis spectrum of complex **16** ($\lambda_{max} = 485$ nm) compared to **6** ($\lambda_{max} = 657$ nm) is qualitatively consistent with the electrochemical results, i.e., higher stabilization of the HOMO in **16** due to dπ(Ru) $\rightarrow \pi^*$(**PCP**−**PCP**) back-donation (HOMO−LUMO gap, $\Delta E = 2.08$ eV) compared to **6** (HOMO−LUMO gap, $\Delta E = 1.90$ eV).

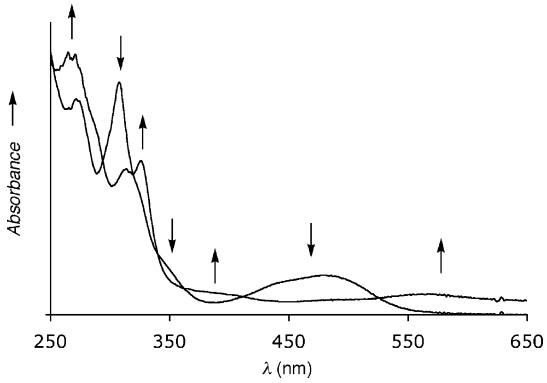

Figure 5. UV−vis spectra recorded before and after complete one-electron oxidation of the mononuclear complex [Ru^{II}(PCP)(tpy)]$^+$ (**19**) to [Ru^{III}-(PCP)(tpy)]$^{2+}$ (**19**$^+$). Conditions: OTTLE cell, $T = 293$ K, MeCN/3 × 10^{-1} M TBAH.

UV−vis spectroelectrochemical measurements with complex **16** were performed in MeCN at room temperature using an optically transparent thin-layer electrochemical (OTTLE) cell[22] to obtain accurate reference electronic absorption spectra of the oxidized species and probe the stability of the complex in several redox states. One-electron oxidation of **16** to **17** at 0.13 V caused partially decreased intensity of the composed band at 485 nm, consistent with the predominant MLCT character of the electronic transitions involved. The initial UV−vis spectrum of **16** could be restored by back-reduction of **17**, demonstrating the reversibility of the anodic process. A full description of the UV−vis−NIR absorption spectrum of mixed-valence **17** (Figure 4) is given in the next section.

Further oxidation of mixed-valence species **17** to **18** (Figure 3) at −0.04 V caused complete disappearance of the band at 485 nm and appearance of two weak bands at 401 and 460 nm. A weak unresolved absorption in this region is also present in the UV−vis spectrum of the one-electron oxidized mononuclear Ru(III) complex **19**$^+$ (see Figure 5). Similarly to the [Ru^{III}−Ru^{III}] complex **4**,[6] the electronic absorption spectrum of green isoelectronic complex **18** displays a very intense, composed low-energy band centered at 747 nm having most likely a predominant ligand-to-metal charge-transfer (LMCT) character.[5a] In the course of electrolysis, sharp isosbestic points at 297, 324, 378, and 550 nm are maintained, and the stepwise reverse reduction of **18** fully recovers the spectra of **17** and **16**. The results obtained by the spectroelectrochemical study confirm the reversible nature of the anodic processes on a longer time scale than that accessible by cyclic voltammetry.

(21) (a) Sauvage, J.-P.; Collin, J.-P.; Chambron, J.-C.; Guillerez, S.; Coudret, C.; Balzani, V.; Barigelletti, F.; De Cola, L.; Flamigni, L. *Chem. Rev.* **1994**, *94*, 993−1019. (b) Zhou, X.; Ren, A.-M.; Feng, J.-K. *J. Organomet. Chem.* **2005**, *690*, 338−347.

(22) (a) Krejčík, M.; Daněk, M.; Hartl, F. *J. Electroanal. Chem., Interfacial Electrochem.* **1991**, *317*, 179−187. (b) Hartl, F.; Luyen, H.; Nieuwenhuis, H. A.; Schoemaker, G. C. *Appl. Spectrosc.* **1994**, *48*, 1522−1528.

Table 4. NIR Spectral Data for the Mixed-Valence Species [(tpy)Ru^{III}(**PCP**−**PCP**)Ru^{II}(tpy)]$^{3+}$ (**17**) and [(tpy)Ru^{III}(**NCN**−**NCN**)Ru^{II}(tpy)]$^{3+}$ (**5**) Recorded at 298 K in MeCN

	17			**5**
complex	band 1	band 2	band 3	
λ_{max} (nm)	1290	1609	2066	1875[a]
ϵ_{max} (cm^{-1} M^{-1})	555	1984	3982	33 000
ν_{max} (cm^{-1})	7751	6215	4840	5333
$\Delta\nu_{obs}$[b] (cm^{-1})	2424	1879	1267	1616
$\Delta\nu_{calcd}$[c] (cm^{-1})	4231	3789	3343	3509
V_{AB} (eV)	0.023[d]	0.035[d]	0.036[d]	0.33[e,f]
Γ[g]	0.43	0.50	0.62	0.70

[a] Identical with the main component of the composed NIR band. [b] Observed half-height bandwidth ($\Delta\nu_{1/2}$) of the NIR band. [c] Half-height bandwidth calculated from eq 1 in the main text. [d] Coupling parameter calculated from eq 2 in the main text. [e] Coupling parameter calculated from eq 3 in the main text. [Ru^{III}−Ru^{II}] charge-transfer distance $d = r_{AB} = 11$ Å (average value derived from the crystallographic data obtained[6] for [Ru^{II}−Ru^{II}] complexes **4** and **6** and [Ru^{III}−Ru^{III}] complex **8**. [f] Much smaller value $V_{AB} = 0.11$ eV obtained from the Hush formula (eq 2). [g] Delocalization parameter calculated from eq 4 in the main text.

NIR Spectra of Mixed-Valence Species. *Hush Theory.* The NIR spectrum of the mixed-valence complex [(tpy)Ru^{III}(**NCN**−**NCN**)Ru^{II}(tpy)]$^{3+}$ (**5**) displays an intense asymmetric absorption band (Table 4) originating from two closely spaced electronic transitions ($\lambda_{max} = 1875$ nm with a shoulder at 1650 nm) attributed originally to intervalence charge transfer (IVCT) absorption.[6a] The IVCT term corresponds to [Ru^{III}(bridge)Ru^{II}] ↔ [Ru^{II}(bridge)Ru^{III}] isomerization in a valence-localized Class II compound. For complex **5**, the main component of the NIR absorption, with a maximum coinciding with that of the band envelope ($\lambda_{max} = 1875$ nm), is fairly narrow, the experimental half-width $\Delta\nu_{1/2} = 1616$ cm^{-1} being much smaller than the half-width of 3509 cm^{-1} calculated from eq 1 introduced by Hush for Class II mixed-valence systems. This difference in the $\Delta\nu_{1/2}$ values indicates a much stronger electronic delocalization in the complex. In view of its redox properties, the high intensity of the NIR band ($\epsilon_{max} = 3.3 \times 10^4$ M^{-1} cm^{-1}), and negligible solvatochromism, it can be concluded that complex **5** belongs to Class III systems with extensively delocalized frontier orbitals.[2d,e,23] Therefore, the NIR bands are more correctly assigned as charge-resonance bands rather than IVCT transition.

$$\Delta\nu_{1/2} = (2310\nu_{max})^{1/2} \quad (1)$$

One-electron oxidation of **16** in MeCN with one equivalent of [$Ce(OTf)_4$] generates the mixed-valence species [(tpy)Ru^{III}(**PCP**−**PCP**)Ru^{II}(tpy)]$^{3+}$ (**17**), which displays a broad band in the NIR region (Figure 4). The absorption envelope has been deconvoluted into three Gaussian-shaped sub-bands (Figure 4, inset). Further oxidation of **17** by the second equivalent of Ce(IV) resulted in formation of the deep green colored [Ru^{III}−Ru^{III}] complex **18**, its UV−vis spectrum well reproducing the spectroelectrochemical result (Figure 3). The observed complete disappearance of the composed NIR band on the one-electron oxidation of **17** to **18**, accompanied by intense charge transfer absorptions (LMCT) arising in the visible region, clearly demonstrates its association with the mixed-valence state.

The experimental parameters of the three separate NIR electronic transitions of **17** are presented in Table 4. Similarly to **5**, the observed $\Delta\nu_{1/2}$ value for each band is considerably lower than that predicted by Hush theory for Class II systems. Lower bandwidths are usually taken as evidence for a Class III system. However, the fairly low intensity of the bands, with their maxima virtually independent of the solvent, classify **17** as a borderline, nearly delocalized Class II/Class III mixed-valence complex with considerable coupling between the ruthenium centers.[24]

The experimental $\Delta\nu_{1/2}$ and ν_{max} values (Table 4) allow for the estimation of the electronic coupling parameter (V_{AB}) using eq 2 for **5** and eq 3 for **17**, which hold for Class III and Class II/Class III systems, respectively.[24]

$$V_{AB} = \nu_{max}/2 \quad (2)$$

$$V_{AB} = [2.06 \times 10^{-2} (\epsilon_{max}\Delta\nu_{1/2}\nu_{max})^{1/2}/r_{AB}] \quad (3)$$

For a more conclusive assignment of **5** to Class III and **17** to borderline Class II/Class III, we employed the delocalization parameter Γ (eq 4), introduced by Brunschwig et al.[24a] as a useful criterion for determining whether a mixed-valence system is weakly, moderately, or strongly coupled.

$$\Gamma = (1 - \theta) = [1 - (\Delta\nu_{1/2}/(2310\nu_{max})^{1/2})] \quad (4)$$

The value of $\Gamma \approx 0.70$ for complex **5** (Table 4) indeed complies with its assignment to intrinsically delocalized Class III, which agrees with a stronger electronic delocalization compared to **17**.

The results of the Hush analysis point to a decreased electronic coupling between the metal centers in the mixed-valence species by introducing the π-acceptor PPh_2 moieties in the pincer arms of the bridging ligand as a result of a larger delocalization of the unpaired electron in the SOMO of **5** compared to that of **17**. For dinuclear systems featuring frontier orbitals extensively delocalized over the metal centers and the bridging ligand, the reasoning whether the NIR absorption corresponds to charge resonance[25] in Class III and borderline Class II/Class III systems rather than to IVCT transitions,[24a] characteristic of valence-localized (Class II) systems, has a limited value, and quantum mechanical calculations are required to clarify the exact nature of these transitions. As recent studies showed that DFT calculations are valuable in the description of the electronic structure of analogous mixed-valence organometallic systems,[26] we performed an initial DFT and TD-DFT study of the mixed-valence complexes as described in the following section.

(23) Demadis, K. D.; Hartshorn, C. M.; Meyer, T. J. *Chem. Rev.* **2001**, *101*, 2655−2686.

(24) (a) Brunschwig, B. S.; Creutz, C.; Sutin, N. *Chem. Soc. Rev.* **2002**, *31*, 168−184. (b) D'Alessandro, D. M.; Keene, F. R. *Chem. Soc. Rev.* **2006**, *35*, 424−440. (c) Kaim, W.; Lahiri, G. K. *Angew. Chem. Int. Ed.* **2007**, *46*, 1778−1796.

(25) Szeghalmi, A. V.; Erdmann, M.; Engel, V.; Schmitt, M.; Amthor, S.; Kriegisch, V.; Nöll, G.; Stahl, R.; Lambert, C.; Leusser, D.; Stalke, D.; Zabel, M.; Popp, J. *J. Am. Chem. Soc.* **2004**, *126*, 7834−7845.

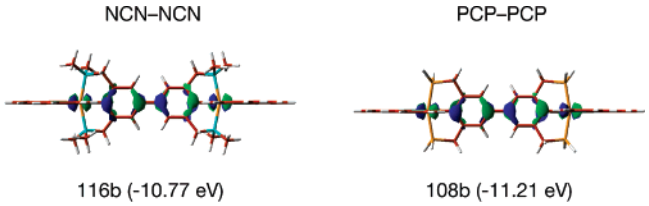

Figure 6. Highest α-occupied MOs of **5** (116b) and **17-H** (108b).

Table 5. Mulliken[28] Spin Population for **5** and **17-H**

group	**5**	**17-H**
Ru(II)/Ru(III)	0.627 (0.314/0.314)	0.552 (0.276/0.276)
biphenylene (C atoms)	0.395	0.463

Table 6. Lowest-Lying Excitations (Δ*E*) in the NIR Spectrum (with $f > 0.001$) for **5** and **17-H** ($c^2 > 0.3$)

	5			**17-H**		
band	Δ*E* (nm) (eV)	f	assignment	ΔE (nm) (eV)	f	assignment
1	1488	0.421	0.52 *β*-115b → *β*-116b	1509	0.644	0.77 *β*-107b → *β*-108b
	(0.83)		0.36 *β*-114b → *β*-116b	(0.82)		
2	1407	0.297	0.64 *β*-114b → *β*-116b	1051	0.019	0.98 *β*-105b → *β*-108b
	(0.88)		0.29 *β*-115b → *β*-116b	(1.18)		

Density Functional Theory. DFT calculations were performed on mixed-valence complex **5** and on the model compound **17-H** containing the bridging ligand $[C_6H_2(CH_2PH_2)_2\text{-}3,5]_2^{2-}$ instead of $[C_6H_2(CH_2PPh_2)_2\text{-}3,5]_2^{2-}$ to reduce the computational efforts. According to the computed DFT results, the unpaired electron in the mixed-valence species is strongly delocalized. Being aware that these results may arise from an artificial preference of DFT methods for delocalization,[27] we performed additional UHF calculations, which have also suggested that oxidation of the biphenylene bridging ligand occurs. The ground-state electronic configurations of the pincer compounds were calculated to be for **5** (NCN) (C_2 symmetry) $((1a)^2(1b)^2...(125a)^2(113b)^2(114b)^2(115b)^2(116b)^1)$ and for **17-H** (PCP) (C_2 symmetry) $((1a)^2(1b)^2...(117a)^2(105b)^2(106b)^2(107b)^2(108b)^1)$. The Mulliken[28] spin population (Table 5) for both compounds shows an equal spin population on both Ru centers and a substantial involvement of the carbon atoms of the bridging biphenylene unit. The fact that the spin population on the Ru centers is higher for **5** than for **17-H** reflects the larger stabilization of the Ru d orbitals in **17** due to the poorer *σ*-donating ability of the **PCP**−**PCP** bridging ligand compared to that of **NCN**−**NCN**, in line with the obtained electrochemical results (i.e., the different anodic electrode potentials of complexes **6** and **16**, see Table 2). The change in spin population as a result of alteration of the relative energetic positions of the Ru d orbitals by the donating ability of the bridging ligand can be rationalized in terms of a simple orbital correlation diagram argument. The highest occupied α orbitals (116b for **5**, 108b for **17-H**, Figure 6) in both compounds can be described as the 'antibonding' combination of the *π*-type d orbitals on Ru and the HOMO of an unperturbed biphenylene system. Let us consider the two limiting cases where the Ru d orbitals are much lower or higher in energy than the HOMO of an unperturbed biphenyl. In the former case, the doubly occupied, 'bonding' combination resembles the Ru d orbitals while the singly occupied, 'antibonding' combination is similar to the unperturbed biphenyl HOMO; in the latter case, the situation is reversed. Thus, rising the Ru d-orbital energy leads to more pronounced Ru d character of the singly occupied orbital and consequently to a higher spin population on the metals.

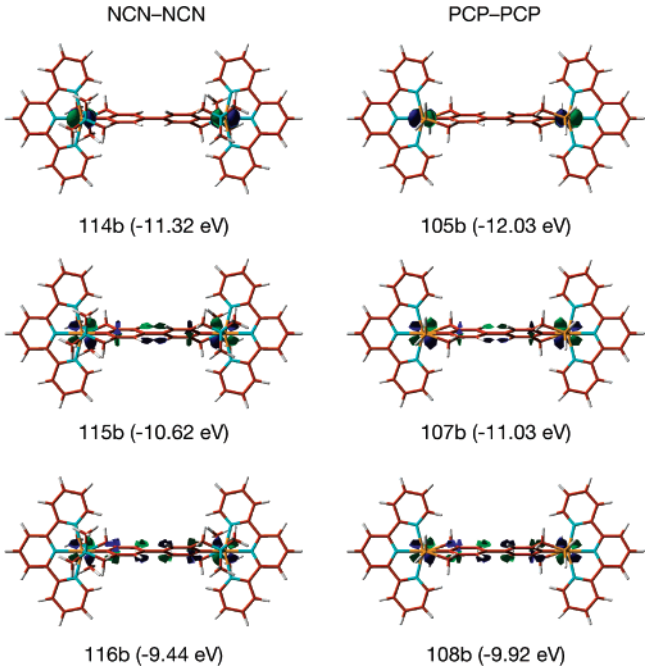

Figure 7. Contour plots of the frontier orbitals of **5** and **17-H** involved in the NIR electronic transitions presented in Table 6.

The near equality of the ruthenium centers thwarts the assignment of the observed near-infrared bands as IVCT transitions. Consequently, these bands were assigned on the basis of TD-DFT calculations. Table 6 presents the characters of the lowest-lying calculated NIR transitions with oscillator strength (*f*) larger than 0.001. The calculated excitation energies are in reasonable agreement with the experimental NIR absorption maxima of **5** and **17** (Table 3), although overestimated.

For both compounds, the lowest-lying bands correspond to excitation of a *β* electron to the singly occupied orbital. The experimental band observed at 1875 nm for **5** may be attributed to the two bands calculated at 1488 and 1407 nm and those at 2066 and 1609 nm in the NIR spectrum of **17** to the transitions calculated for **17-H** at 1509 and 1051 nm. The TD-DFT calculations do not predict the band at 1290 nm obtained by deconvolution of the NIR band of **17**.

(26) (a) Röder, J. C.; Meyer, F.; Hyla-Kryspin, I.; Winter, R. F.; Kaifer, E. *Chem. Eur. J.* **2003**, *9*, 2636−2648. (b) van Slageren, J.; Winter, R. F.; Hartmann, S. *J. Organomet. Chem.* **2003**, *670*, 137−143. (c) Mauer, J.; Winter, R. F.; Sarkar, B.; Fiedler, J.; Záliš, S. *Chem. Commun*. **2004**, 1900−1901. (d) Bühl, M.; Thiel, W. *Inorg. Chem*. **2004**, *43*, 6377−6382.

(27) (a) Sodupe, M.; Bertran, J.; Rodríguez-Santiago, L.; Baerends, E. J. *J. Phys. Chem. A* **1999**, *103*, 166−170. (b) Grüning, M; Gritsenko, O. V.; van Gisbergen, S. J. A.; Baerends, E. J. *J. Phys. Chem. A* **2001**, *105*, 9211−9218.

(28) Mulliken, R. S. *J. Chem. Phys*. **1955**, *23*, 1833−1840.

Therefore, we surmise that the broadness of the NIR band in **17** is probably due to an unresolved vibrational progression.[27]

Plots of the frontier orbitals of **5** and **17-H** involved in the NIR transitions (Figure 7) give an indication of the charge transfer upon excitation. The β-HOMO (115b), HOMO−1 (114b), and β-LUMO (116b) of **5** reside on the metal and the π orbitals of the bridging ligand. The β-HOMO (107b) of **17-H** is mainly localized on the metal with tails on the bridging ligand, while the β-HOMO-2 (105b) is mainly metal in character. The NIR absorption bands for both complexes are thus not originated by a single IVCT transition, as previously proposed,[5,6] but are composed of transitions with a predominant MLCT and some minor LMCT character. A more in-depth theoretical study is currently in progress to resolve the discrepancies between theory and experiment and the effect of the preference of DFT for a delocalized state on the calculated transition energies and assignments.

Conclusions

In contrast to the mononuclear complex $[Ru^{II}(NCN)(tpy)]Cl$, reaction of $[Ru^{II}(PCP)(tpy)]Cl$ with an excess of $CuCl_2$ does not result in smooth formation of a dinuclear Ru(III) species. Therefore, synthesis of the $[(tpy)Ru^{II}(\mathbf{PCP}-\mathbf{PCP})Ru^{II}(tpy)]Cl_2$ complex was carried out by a selective double transcyclometalation of the pincer ligand $[C_6H_3(CH_2PPh_2)_2\text{-}3,5]_2$, abbreviated as [**PC(H)P**−**PC(H)P**], with the ruthenium precursor $[RuCl(NCN)(PPh_3)]$ followed by coordination of ancillary terpyridine ligands. The electrochemical and spectroscopic properties of $[(tpy)Ru^{II}(\mathbf{PCP}-\mathbf{PCP})Ru^{II}(tpy)]Cl_2$ were investigated and compared with those of the related complex $[(tpy)Ru^{II}(\mathbf{NCN}-\mathbf{NCN})Ru^{II}(tpy)](PF_6)_2$. One-electron reduction of $[(tpy)Ru^{III}(\mathbf{NCN}-\mathbf{NCN})Ru^{III}(tpy)](PF_6)_4$ and one-electron oxidation of $[(tpy)Ru^{II}(\mathbf{PCP}-\mathbf{PCP})Ru^{II}(tpy)]Cl_2$ lead to formation of the mixed-valence species $[(tpy)Ru^{III}(\mathbf{NCN}-\mathbf{NCN})Ru^{II}(tpy)]^{3+}$ and $[(tpy)Ru^{III}(\mathbf{PCP}-\mathbf{PCP})Ru^{II}(tpy)]^{3+}$, respectively. Both products absorb strongly in the NIR spectral region. Analysis of the features of the NIR absorption bands by Hush theory shows that the mixed-valence species $[(tpy)Ru(\mathbf{PCP}-\mathbf{PCP})Ru(tpy)]^{3+}$ belongs to borderline Class II/Class III (nearly delocalized) systems ($\Gamma \approx 0.5$). The complex $[(tpy)Ru(\mathbf{NCN}-\mathbf{NCN})Ru(tpy)]^{3+}$ is an intrinsically delocalized Class III compound ($\Gamma \approx 0.7$). Clearly, for both mixed-valence species the extensively delocalized bonding situation excludes the assignment of the NIR bands to IVCT transitions, as suggested for $[(tpy)Ru^{III}(\mathbf{NCN}-\mathbf{NCN})Ru^{II}(tpy)]^{3+}$ in the literature. Delocalization in both complexes has been predicted by DFT calculations, which document an equal spin population of both Ru centers. TD-DFT calculations have suggested that the low-lying NIR bands can be assigned as predominantly MLCT in character.

The results of this study show that the 'soft' donor and π-acceptor PPh_2 moieties in the pincer arms of the **PCP**−**PCP** ligand bridge attenuate the delocalization of the unpaired electron in the mixed-valence species. In general, fine-tuning of the electronic coupling can be achieved by modification of the donor characteristics of the pincer arms of the bridging ligand. The ancillary terpyridine ligands are not important in this regard as their cathodic responses remain unaffected in the studied series of mono- and dinuclear complexes (Table 2). The facile preparation of this class of complexes and their stability to air, moisture, and high temperatures (decomposition above 350 °C) represent their additional advantageous characteristics together with the fast and selective interconversion between the $[Ru^{III}-Ru^{III}]$, formally $[Ru^{III}-Ru^{II}]$, and $[Ru^{II}-Ru^{II}]$ redox forms. The results obtained are encouraging for future development of these species directed toward photochromic devices. Moreover, the possibility to introduce substituents at the 4′-position of the terminal terpyridine ligands opens the possibility to explore the anchoring of these complexes on materials such as polymers, dendrimers, and semiconductor surfaces to form larger supramolecular architectures.

Experimental Section

General. All experiments were carried out under an atmosphere of dry nitrogen using standard Schlenk techniques. Benzene, toluene, pentane, hexane, and Et_2O were distilled from sodium/benzophenone. CH_2Cl_2 was dried over CaH_2, MeOH over magnesium, and MeCN over P_2O_5. All solvents were freshly distilled under nitrogen prior to use. NMR spectra [^1H (300.1 MHz), ^{13}C (75.5 MHz), and $^{31}P\{^1H\}$ (121.4 MHz)] were recorded on a Varian Inova 300 MHz spectrometer. Chemical shifts are given in ppm relative to the residual solvent signal (^1H and ^{13}C NMR spectra) or 85% H_3PO_4 external reference ($^{31}P\{^1H\}$ NMR spectra). All reagents were purchased from Acros Chemicals or Aldrich and used as received. Compounds **1**,[12] **14**,[12] and **19**[14] were synthesized according to literature procedures. Elemental analyses were performed by Dornis and Kolbe, Mikroanalytisches Laboratorium, Mülheim a. d. Ruhr, Germany. High-resolution electrospray ionization (ESI) mass spectra were recorded with a Micromass LC-TOF mass spectrometer at the Biomolecular Mass Spectrometry group, Utrecht University.

Electrochemical Measurements. Cyclic and square-wave voltammetric scans were performed with a gastight single-compartment cell under an atmosphere of dry nitrogen. The cell was equipped with Pt microdisk working (apparent surface area of 0.42 mm^2), Pt wire auxiliary, and Ag wire pseudoreference electrodes. The working electrode was carefully polished with a 0.25 μm grain diamond paste between scans. The potential control was achieved with a PAR Model 283 potentiostat. All redox potentials are reported against the ferrocene/ferrocenium (Fc/Fc^+) redox couple used as an internal standard ($E_{1/2} = +0.63$ V vs NHE).[30,31] Bu_4NPF_6 (3×10^{-1} M; TBAH) was used as supporting electrolyte. All electrochemical samples were 5×10^{-4} M in the studied complexes.

Electronic Absorption Spectroscopy. UV−vis spectra were obtained on a Varian Cary 1 spectrophotometer using matched 1 cm quartz cells (Hellma) and operating with 0.5 nm spectral resolution.

UV−vis Spectroelectrochemistry. All experiments were performed with an optically transparent thin-layer electrochemical (OTTLE) cell[22] equipped with a Pt minigrid working electrode and quartz optical windows. The controlled-potential electrolyses were

(29) Adams, S. J.; Fey, N.; Parfitt, M.; Pope, S. J. A.; Weinstein, J. A. *Dalton Trans.* **2007**, 4446−4456.
(30) Pavlishchuk, V. V.; Addison, A. W. *Inorg. Chim. Acta* **2002**, *298*, 97−102.
(31) Gritzner, G.; Kůta, J. *Pure Appl. Chem.* **1984**, *56*, 461−466.

carried out with a PA4 potentiostat (EKOM, Polná, Czech Republic). All electrochemical samples were 5×10^{-4} M in the studied complex and contained 3×10^{-1} M Bu_4NPF_6. In situ UV−vis spectra were recorded on a Hewlett-Packard 8453 diode-array spectrophotometer.

X-ray Crystal Structure Determination of Complex 4. $[C_{54}H_{58}N_{10}Ru_2](PF_6)_4$ + disordered solvent, $M_w = 1629.12$ [derived values do not contain the contribution from the disordered solvent molecules], orange plate, $0.24 \times 0.24 \times 0.06$ mm, triclinic, $P\bar{1}$ (no. 2), $a = 16.5095(1)$ Å, $b = 17.6890(1)$ Å, $c = 18.5598(2)$ Å, $\alpha = 97.2109(4)°$, $\beta = 110.7621(4)°$, $\gamma = 116.6773(5)°$, $V = 4257.69(7)$ Å^3, $Z = 2$, $D_x = 1.271$ g cm^{-3} [derived values do not contain the contribution from the disordered solvent molecules], $\mu = 0.52$ mm^{-1} [derived values do not contain the contribution from the disordered solvent molecules]. There were 64 494 reflections measured on a Nonius Kappa CCD diffractometer with rotating anode (graphite monochromator, $\lambda = 0.71073$ Å) up to a resolution of $(\sin \theta/\lambda)_{max} = 0.60$ Å^{-1} at $T = 150$ K. An absorption correction based on multiple measured reflections was applied (0.92−0.98 correction range). A total of 15 366 reflections were unique ($R_{int} = 0.0657$). The structure was solved with automated Patterson methods[32] and refined with SHELXL-97[33] against F^2 of all reflections. Non-hydrogen atoms were refined with anisotropic displacement parameters. All hydrogen atoms were introduced in geometrically idealized positions and refined with a riding model. The crystal structure contains large voids (1449.8 Å^3/unit cell) filled with disordered solvent molecules. Their contribution to the structure factors was secured by back-Fourier transformation using the SQUEEZE routine of the PLATON program,[34] resulting in 431 electrons/unit cell. A total of 855 parameters were refined with no restraints. *R*1/*wR*2 [$I > 2\sigma(I)$]: 0.0398/0.0903. *R*1/*wR*2 [all reflns]: 0.0573/0.0959. $S = 0.958$. Residual electron density between −0.67 and 1.44 e Å^{-3}. Geometry calculations and checking for higher symmetry were performed with the PLATON program.[34]

Computational Details. Geometries of **5** (C_2) and **1-H** (C_2) were optimized with GAMESS-UK[35] at the UB3LYP level of theory using the Stuttgart 1997 ECP for Ru and the 6-31G** basis set for all other atoms. TD-DFT calculations were performed with GAUSSIAN 03[36] using the same basis set.

[(tpy)Ru^{III}(NCN−NCN)Ru^{III}(tpy)](PF$_6$)$_4$ (4). A dark blue solution of **1** (0.13 g, 0.25 mmol) in dry MeOH (10 mL) turned red immediately after addition of $CuCl_2$ (0.8 g, 0.6 mmol). The mixture was stirred at reflux for 5 h, after which time the solvent was removed in vacuo. The green residue was redissolved in MeCN (3 mL), and the solution was treated with an excess of aqueous NH_4PF_6. The obtained precipitate was washed with water and subjected to silica gel column chromatography (elution with MeCN/H_2O/satd aq. KNO_3 (6:3:1 v/v)). Removal of the solvents from the first and second eluted fractions gave **3** (7%) and **4** (yield: 0.34 g, 85%) as red and green solids, respectively. Single copper-colored crystals of **4** suitable for X-ray diffraction analysis were obtained by slow evaporation of a solution of **4** in MeCN (2 mL) containing toluene (5 mL). ^{1}H NMR (300 MHz, CD_3CN): δ 8.92 (d, $^1J_{HH} = 8.11$ Hz, 4H, tpy(3′, 5′)), 8.77 (d, $^1J_{HH} = 6.6$ Hz, 2H, tpy(6, 6″)), 8.76 (s, 4H, Ar), 8.59 (t, $^1J_{HH} = 8.1$ Hz, 2H, tpy(4′)), 8.22 (d, $^2J_{HH} = 7.0$ Hz, 4H, tpy(3, 3″)), 8.21 (t, $^1J_{HH} = 8.39$ Hz, 4H, tpy(4, 4″)), 7.62 (t, $^1J_{HH} = 6.45$ Hz, 4H, Pyr(5, 5″)), 4.01 (s, 8H, CH_2), 1.28 (s, 24H, NCH_3). ^{13}C NMR (75 MHz, $CDCl_3$): δ 158.1, 157.9, 153.8, 148.8, 142.6, 142.5, 142.0, 129.9, 129.3, 127.1, 124.3, 114.0, 74.8 (NCH_3), 53.83 (CH_2). Anal. Calcd for $C_{54}H_{58}F_{24}N_{10}P_4Ru_2$: C, 39.81; H, 3.59; N, 8.60. Found: C, 39.75; H, 3.68; P, 8.55.

[3,5-Bis(methoxymethyl)pinacolboranebenzene] (9). Magnesium lumbs (1.56 g, 64.2 mmol) were stirred vigorously under a nitrogen atmosphere in a three-necked round-bottom flask for 1 h followed by addition of THF (10 mL). A few drops of **7** (or alternatively 1,2-dichloroethane) were added to start the reaction. A solution of **7** (9.38 g, 32.11 mmol, 0.5 equiv) in THF (90 mL) was then added dropwise. During the addition the solution turned dark gray. After the addition was complete, the mixture was stirred at room temperature for 3 h and subsequently heated (ca. 15 h) to reflux until full conversion of **7** to **8** was reached. The conversion of **7** was determined by ^{1}H NMR spectroscopy by analyzing aliquots of the mixture quenched with S_2Me_2. The obtained solution was filtered to remove the excess Mg and diluted by adding THF (100 mL). After addition of $B(OMe)_3$ (7.5 mL, 65.7 mmol, 1.0 equiv), the obtained mixture was heated at 50 °C for 15 h. Next, pinacol (4.15 g, 0.55 equiv) was added at room temperature, followed by AcOH (0.5 equiv) after 10 min. The reaction mixture was stirred at room temperature for 1 h and then evaporated to dryness, and Et_2O (200 mL) was added. The precipitated salts were removed by filtration. Removal of the solvent in vacuo gave **9** as yellow oil. Yield: 9.16 g, 98%. ^{1}H NMR (300 MHz, $CDCl_3$): δ 7.69 (s, 2H, Ar), 7.45 (s, 1H, Ar), 4.49 (s, 4H, CH_2), 3.38 (s, 6H, OCH_3), 1.38 (s, 12H, CCH_3). ^{13}C NMR (75 MHz, $CDCl_3$): δ 137.9, 133.7, 130.2, 127.12, 83.9 (OCH_3), 74.7 (CH_2), 58.3 (CCH_3), 25.0 (CH_3). Anal. Calcd for $C_{16}H_{25}BO_4$: C, 65.77; H, 8.62. Found: C, 65.85; H, 8.56.

[C$_6$H$_3$(CH$_2$OMe)$_2$-3,5]$_2$ (10). A mixture of **7** (2.56 g, 8.8 mmol), **9** (2.56 g, 8.8 mmol), Na_2CO_3 (2.23 g, 21.0 mmol), and [$PdCl_2$(dppf)] (0.16 g, 0.23 mmol) in degassed DMF/THF/H_2O (1:1:1 v/v) (120 mL) was heated at 50 °C for 15 h under a nitrogen atmosphere. The organic products formed were extracted with Et_2O (2×70 mL). Evaporation of the solvent gave crude **10** as a brown oil (containing 10% of **7**) that was purified by column chromatography (silica, pentane/Et_2O (3:7 v/v)). Yield: 1.97 g, 68%. ^{1}H NMR (300 MHz, $CDCl_3$): δ 7.51 (s, 4H, Ar), 7.29 (s, 2H, Ar), 4.52 (s, 8H, CH_2), 3.42 (s, 12H, OCH_3). ^{13}C NMR (75 MHz, $CDCl_3$): δ 141.4, 139.2, 126.2, 126.0, 74.8, 58.4 (CH_2). Anal. Calcd for $C_{20}H_{26}O_4$: C, 72.70; H, 7.93. Found: C, 72.87; H, 7.95.

[C$_6$H$_3$(CH$_2$Br)$_2$-3,5]$_2$ (11). A mixture of **10** (5.29 g, 1.6 mmol), $BF_3{\cdot}Et_2O$ (30 g, 2.17 mmol), and AcBr (31.5 g, 2.56 mmol) in CH_2Cl_2 (150 mL) was stirred at reflux for 18 h. The mixture was then cooled to 0 °C by an ice bath. Next, saturated aqueous K_2CO_3 solution was added slowly until no evolution of gas was observed.

(32) Beurskens, P. T.; Admiraal, G.; Beurskens, G.; Bosman, W. P.; Garcia-Granda, S.; Gould, R. O.; Smits, J. M. M.; Smykalla C. *The DIRDIF99 program system*; Technical Report of the Crystallography Laboratory; University of Nijmegen: The Netherlands, 1999.

(33) Sheldrick, G.M. *SHELXL-97, Program for crystal structure refinement*; University of Göttingen: Göttingen, Germany, 1997.

(34) Spek, A. L. *J. Appl. Crystallogr.* **2003**, *36*, 7−13.

(35) Guest, M. F.; Bush, I. J.; van Dam, H. J. J.; Sherwood, P.; Thomas, J. M. H.; van Lenthe, J. H.; Havenith, R. W. A.; Kendrick, J. *Mol. Phys.* **2005**, *103*, 719−747.

(36) Frisch, M. J.; Trucks, G. W.; Schlegel, H. B.; Scuseria, G. E.; Robb, M. A.; Cheeseman, J. R.; Montgomery, J. A.; Vreven, Jr., T.; Kudin, K. N.; Burant, J. C.; Millam, J. M.; Iyengar, S. S.; Tomasi, J.; Barone, V.; Mennucci, B.; Cossi, M.; Scalmani, G.; Rega, N.; Petersson, G. A.; Nakatsuji, H.; Hada, M.; Ehara, M.; Toyota, K.; Fukuda, R.; Hasegawa, J.; Ishida, M.; Nakajima, T.; Honda, Y.; Kitao, O.; Nakai, H.; Klene, M.; Li, X.; Knox, J. E.; Hratchian, H. P.; Cross, J. B.; Adamo, C.; Jaramillo, J.; Gomperts, R.; Stratmann, R. E.; Yazyev, O.; Austin, A. J.; Cammi, R.; Pomelli, C.; Ochterski, J. W.; Ayala, P. Y.; Morokuma, K.; Voth, G. A.; Salvador, P.; Dannenberg, J. J.; Zakrzewski, V. G.; Dapprich, S.; Daniels, A. D.; Strain, M. C.; Farkas, O.; Malick, D. K.; Rabuck, A. D.; Raghavachari, K.; Foresman, J. B.; Ortiz, J. V.; Cui, Q.; Baboul, A. G.; Clifford, S.; Cioslowski, J.; Stefanov, B. B.; Liu, G.; Liashenko, A.; Piskorz, P.; Komaromi, I.; Martin, R. L.; Fox, D. J.; Keith, T.; Al-Laham, M. A.; Peng, C. Y.; Nanayakkara, A.; Challacombe, M.; Gill, P. M. W.; Johnson, B.; Chen, W.; Wong, M. W.; Gonzalez, C.; Pople, J. A. *Gaussian 03*, Revision B.05; Gaussian, Inc.: Pittsburgh, PA, 2003.

Subsequently, the collected organic layer was dried over $MgSO_4$, filtered, and concentrated to 5 mL. Hexane was added slowly, resulting in precipitation of pure **11** as white crystals, which were collected by filtration and dried in vacuo. Yield: 5.48 g, 65.0%. ^{1}H NMR (300 MHz, $CDCl_3$): δ 7.52 (s, 4H, Ar), 7.44 (s, 2H, Ar), 4.55 (s, 8H, CH_2). ^{13}C NMR (75 MHz, $CDCl_3$): δ 141.4, 139.4, 129.2, 128.0, 32.8 (CH_2). Due to its toxicity, elemental and ESI analyses of **11** were not carried out. *Caution: benzylic bromides can act as powerful lachrymators and should be used with adequate ventilation and precaution against skin contact or ingestion.*

[C$_6$H$_3$(CH$_2$PPh$_2$)$_2$-3,5]$_2$ ([PC(H)P−PC(H)P]) (13). *n*BuLi (3.5 mL, 5.5 mmol, 1.6 M in hexane) was added under stirring to a solution of $HPPh_2$·BH_3 (1.1 g, 5.5 mmol) in THF (80 mL) cooled to −78 °C. The temperature was then allowed to rise to 293 K, and stirring was continued for another 15 h. Subsequently, a solution of **11** (0.73 g, 1.4 mmol) in THF (30 mL) was added at −78 °C. The mixture was then stirred for another 18 h at room temperature. All volatiles were evaporated, and the obtained residue was dissolved in Et_2O. The organic layer was washed with H_2O, dried over $MgSO_4$, and concentrated until only a few milliliters remained. The precipitated white solid was collected, redissolved in a few milliliters of CH_2Cl_2, and filtered. Addition of EtOH caused precipitation of **11** (Scheme 4) as a white solid that was collected by filtration, washed with hexane, and dried in vacuo. Yield: 0.93 g, 67.4%. ^{1}H NMR (300 MHz, $CDCl_3$): δ 7.59−7.56 (m, 22H, Ar + PAr_2), 7.49−7.25 (m, 24H, PAr_2), 3.41 (d, $^2J_{HP}$ = 11.7 Hz, 8H, CH_2), 0.90 (br s, 12H, BH_3). ^{13}C NMR (75 MHz, $CDCl_3$) δ 139.8−127.94 (Ar + PAr_2), 34.07 (d, $^2J_{CP}$ = 32.9 Hz, CH_2). ^{31}P{^{1}H} NMR (121.4 MHz, $CDCl_3$): δ 18.9 (s). Anal. Calcd for $C_{64}H_{66}B_4P_4$: C, 76.69; H, 6.64; P, 12.36. Found: C, 76.78; H, 6.53; P, 12.26.

Removal of BH$_3$. HBF_4·Et_2O (5 mL, 13.2 mmol) was added under a nitrogen atmosphere to a stirred solution of **12** (0.2 g, 0.2 mmol) in CH_2Cl_2 at 0 °C. The temperature was then allowed to rise to 293 K, and stirring was continued for another 18 h. A saturated aqueous $NaHCO_3$ solution was added dropwise at 0 °C, resulting in a considerable gas evolution. When the addition was complete, the mixture was stirred at room temperature for another 1 h. The organic layer was collected and dried over $MgSO_4$. After evaporation of all the volatiles, **13** was obtained as an air- and a moisture-sensitive white sticky solid. Yield: 0.140 g, 80%. ^{1}H NMR (300 MHz, $CDCl_3$): δ 7.43−7.32 (m, 40H, PAr_2), 6.84 (s, 4H, Ar), 6.60 (s, 2H, Ar), 3.34 (s, 8H, CH_2). ^{31}P{^{1}H} NMR (121.4 MHz, $CDCl_3$): δ −8.6 (s).

[{RuCl(PPh$_3$)}$_2$(4,4′-{C$_6$H$_2$(CH$_2$PPh$_2$)$_2$-2,6}$_2$] (15). A solution of **13** (0.140 g, 0.15 mmol) in C_6H_6 (20 mL) was added to a solution of **14** (0.17 g, 0.15 mmol) in C_6H_6 (10 mL). The reaction mixture was stirred at room temperature for 2 days. The solvent was removed in vacuo till only a small residual amount remained. Addition of hexane caused precipitation of an air- and a moisture-sensitive deep green solid that was collected by filtration on a glass filter and washed with cold hexane. Yield: 0.21 g, 70%. ^{1}H NMR (300 MHz, $CDCl_3$): δ 7.77−7.37 (m, 18H, Ar), 7.07−7.66 (m, 64H, Ar + PAr_2), 3.46 (dvt, $^2J_{HH}$ = 15.6 Hz, $^2J_{HP}$ = 6.0 Hz, 4H, CH_2), 2.49 (br d, $^2J_{HH}$ = 16.5 Hz, 4H, CH_2). ^{31}P{^{1}H} NMR (80.91 MHz, $CDCl_3$): δ 82.6 (t, $^2J_{PP}$ = 30.0 Hz, PPh_3), 37.5 (d, $^2J_{PP}$ = 31.5 Hz, PCP). Anal. Calcd for $C_{100}H_{82}Cl_2P_6Ru_2$·$2CH_2Cl_2$: C, 64.06; H, 4.53; P, 9.72. Found: C, 63.90; H, 4.64; P, 9.22.

[(tpy)Ru^{II}(PCP−PCP)Ru^{II}(tpy)]Cl$_2$ (16). A solution of 2,2′:6′,2″-terpyridine (0.05 g, 0.2 mmol) was added in one portion to deep green **15** (0.21 g, 0.1 mmol). The mixture was stirred at reflux temperature for 3 days, during which time the color of the solution turned dark orange. The solvent was removed in vacuo until a small residual amount remained. Addition of Et_2O resulted in precipitation of **16** as an orange air-stable solid. The latter was collected by centrifugation, washed with hexane, and dried in vacuo. The crude product was further purified by column chromatography (silica, MeCN/H_2O (8.5:1.5 v/v)). Yield: 0.112 g, 66.6%. ^{1}H NMR (300 MHz, CD_3OCD_3): δ 9.08 (d, $^1J_{HH}$ = 7.8 Hz, 4H, tpy(3′, 5′)), 8.63 (d, $^1J_{HH}$ = 8.6 Hz, 2H, tpy(6, 6″)), 8.47 (t, $^1J_{HH}$ = 7.95 Hz, 2H, tpy(4′)), 8.20 (s, 4H, Ar), 7.65 (t, $^1J_{HH}$ = 7.65 Hz, 4H, tpy(4, 4″)), 7.56 (d, $^2J_{HH}$ = 5.0 Hz, 4H, tpy(3, 3″)), 7.16 (vt, $^1J_{HH}$ = 8.2 Hz, 8H, *para*-H PAr_2), 7.02 (vt, $^1J_{HH}$ = 7.30 Hz, 16H, *ortho*-H PPh_2), 6.83 (t, $^1J_{HH}$ = 6.0 Hz, 4H, tpy(5, 5″)), 6.74 (m, 8H, *meta*-H PAr_2), 4.00 (vt, 8H, $^1J_{HP}$ = 3.0 Hz, CH_2−P). ^{31}P{^{1}H} NMR (81.91 MHz, CD_3OCD_3): δ = 43.1 (s). Anal. Calcd for $C_{94}H_{74}Cl_2N_6P_4Ru_2$: C, 67.02; H, 4.43; N, 4.99; P, 7.35. Found: C, 66.75; H, 4.36; N, 5.10; P, 7.22.

[C$_6$H$_3$(CH$_2$NMe$_2$)$_2$-3,5]$_2$ ([NC(H)N−NC(H)N]) (21). Neat $NHMe_2$ (20 mL, 280 mmol) was added under stirring to a solution of **11** (2.69 g, 5.1 mmol) in CH_2Cl_2 (40 mL) cooled to 0 °C. The temperature of the reaction mixture was allowed to rise to 293 K, and stirring was continued for 15 h, after which aqueous NaOH (50 mL, 4 M) was added. The CH_2Cl_2 fraction was collected, washed with saturated aqueous NaCl (50 mL), dried over $MgSO_4$, and filtered. Evaporation of the filtrate gave product **21** as a yellow oil, which was further purified by column chromatography (alumina, CH_2Cl_2, 3% NEt_3). Yield: 1.35 g, 70%. NMR data of the obtained compound were consistent with values reported elsewhere.[17]

[C$_6$H$_2$Li-4-(CH$_2$NMe$_2$)$_2$-3,5]$_2$ (22). *t*BuLi (2.76 mL, 4.14 mmol, 1.5 M in pentane) was added under stirring to a solution of **21** (0.63 g, 1.8 mmol) in Et_2O at −78 °C. The resulting orange suspension was allowed to warm to room temperature and stirred for another 14 h. Off-white crystals of **22**, obtained upon cooling to −30 °C, were separated by the pale yellow Et_2O layer. They were collected, washed with cold Et_2O, and dried in vacuo. Yield: 0.4 g, 55.0%. Due to its high flammability, compound **22** was used directly in the following reaction without further purification.

[(tpy)Ru^{II}(NCN−NCN)Ru^{II}(tpy)](PF$_6$)$_2$ (6). A solution of [$RuCl_2(PPh_3)_3$] (0.76 g, 0.8 mmol) in THF (20 mL) was slowly added at room temperature under vigorous stirring to a solution of **22** (0.16 g, 0.4 mmol) in THF (20 mL). The color of the mixture turned rapidly dark blue, consistent with formation of the dinuclear complex **23** (Scheme 6). After stirring for another 5 h, the volatiles were removed in vacuo and a solution of 2,2′:6′,2″-terpyridine (0.19 g, 0.8 mmol) was added in one portion. The resulting mixture was stirred at reflux for 6 h. Next, the solvent was removed in vacuo, and the blue residue was washed with pentane and redissolved in MeCN (5 mL). Addition of an excess of aqueous NH_4PF_6 caused precipitation of **6** as a dark blue solid that was collected, washed with water, and dried in vacuo. Yield: 0.16 g, 15%. NMR data of product **6** are consistent with the previously reported values for **6** prepared according to the synthesis route presented in Scheme 1.[6b]

Acknowledgment. The authors kindly acknowledge Dr. S. Gracea-Tanase and Dr. E. Bouwman from the University of Leiden for having performed EPR and magnetic susceptibility measurements on complex **4**. NWO/NCF is thanked for the supercomputer time on TERAS/ASTER, SARA (The Netherlands, Project No. SG-032). This work was supported by the Council for Chemical Sciences of the Dutch Organization for Scientific Research (NWO). R.W.A.H. acknowledges financial support from the NWO Grant 700.53.401.

IC701501Q